A Rare Example of Four-Coordinate Nonoxido Vanadium(IV) Alkoxide in the Solid State: Structure, Spectroscopy, and Magnetization Dynamics

(Article begins on next page)

A rare example of four-coordinate non-oxido vanadium(IV) alkoxide in the solid state: structure, spectroscopy and magnetization dynamics

Danilo Stinghen,[a] Matteo Atzori,[b] Caprici M. Fernandes,[a] Ronny R. Ribeiro,[a] Eduardo L. de Sá,[a] Davi F. Back,[c] David L. Hughes,[d] Giovana G. Nunes,[a] Mario Chiesa,[e] Renato Torre,[e] Roberta Sessoli[b] and Jaísa F. Soares[a,*]

[a]*Departamento de Química, Universidade Federal do Paraná, Centro Politécnico, Jardim das Américas, 81530-900 Curitiba-PR, Brazil*

[b] *Dipartimento di Chimica "Ugo Schiff" and INSTM RU, Università degli Studi di Firenze, Via della Lastruccia 3, 50019 Sesto Fiorentino (FI), Italia*

[c] *Departamento de Química, Universidade Federal de Santa Maria, Camobi, 97105-900 Santa Maria-RS, Brazil*

[d] *School of Chemistry, University of East Anglia, Norwich NR4 7TJ, UK*

[e] *Dipartimento di Chimica e NIS Centre, Università di Torino, Via P. Giuria 7, I10125 Torino, Italia*

Correspondence to: J. F. Soares (e-mail: jaisa@quimica.ufpr.br)

Abstract

The distorted tetrahedral [V(OAd)$_4$] alkoxide (OAd = 1-adamantoxide, complex **1**), is the first homoleptic, mononuclear vanadium(IV) alkoxide to be characterised in the solid state by X-ray diffraction analysis. The compound crystallises in the cubic $P\bar{4}3n$ space group with two highly disordered, crystallographically independent molecules in the asymmetric unit. Spin Hamiltonian parameters extracted from electron paramagnetic resonance (EPR) spectra registered at 77 K ($g_z < g_x \approx g_y$ and $A_z >> A_x \approx A_y$) have been compared with X-ray and literature data to shade light into the electronic structure of **1**. [V(OAd)$_4$] has also been characterized by AC susceptometry with varying temperature (3-30 K) and static magnetic field (up to 8.5 T), showing field-induced slow relaxation of the magnetization with relaxation times ranging from *ca* 3 ms at 3 K to 0.02-0.03 ms at 30 K, in line with relevant results described recently for other potential molecular quantum bits. This slow spin relaxation is the first observed for a tetracoordinate non-oxido vanadium(IV) complex, and results are compared here to those generated by square-pyramidal $V^{IV}(O)^{2+}$ and trigonal prismatic V^{4+} with oxygen donor atom sets. Considering that the number of promising d^1 complexes investigated in detail for slow magnetization dynamics is still small, the present work contributes to the establishment of possible structural/electronic correlations of interest to the field of quantum information processing.

INTRODUCTION

Oxidovanadium(IV) complexes have been extensively studied for many years because of their relatively easy syntheses, structural variety, catalytic,[1-3] electrochemical[4] and spectroscopic properties[5] and, very recently, remarkable magnetic features as potential molecular quantum bits.[6-11] On the other hand, non-oxido vanadium(IV) compounds are much less common because of the distinctive oxophilicity of the hard "bare" V^{IV} ion, which leads to high tendency towards hydrolysis or oxidation. To explore the still largely unknown spectroscopic and magnetic properties of these elusive complexes, synthetic approaches based on the use of polydentate ligands to block coordination positions around V^{IV}, and therefore make it less reactive, have been employed.[12-15] Chelation, however, establishes geometric constraints and limits available symmetries. Alternatively, bulky monodentate, good $\sigma-$ or $\pi-$donor ligands have been used to shield highly oxidised metal cations and even stabilize unusual electron configurations.[16-18]

Among other classes of high-oxidation-state metal complexes of technological interest, vanadium alkoxides have long been investigated due to their propensity to form high-purity metal oxides under mild conditions, by methods that include chemical or physical vapour deposition (CVD and PVD) or sol-gel processes.[19-22] The rich variety of structural features, useful solubility in organic solvents and high reactivity of these alkoxides also allow for the preparation of heterometallic species, marking them as convenient precursors for the formation of mixed-metal materials with controlled stoichiometry.[23-26] Applications of the strongly basic/reactive character of these alkoxides in organic synthesis and catalysis are also noteworthy.[27-29]

Our research group has extensively surveyed the chemical, structural and spectroscopic features of non-oxido vanadium(IV) species for several reasons. We have employed simple monodentate alkoxides to synthesise "bare" V^{IV} precursors that have been transformed further into nanostructured vanadium oxide materials.[30-32] We have also shown that small alkoxido ligands produce complexes with temperature-dependent dissociation equilibria in solution.[33,34] We have also been involved in the characterisation

of "bare" vanadium(IV) complexes for which an unquenched orbital contribution to the susceptibility may give rise to magnetic anisotropy.[34]

Amongst the scarce well-characterised complexes of non-oxido V^{IV} in coordination numbers lower than six, particularly with monodentate ligands, reports on discrete mononuclear species of tetrahedral geometry are distinctively rare. This is mainly due to the high electron deficiency of these reactive species, which tends to favour polynuclear aggregation. Inspired by an early report from Bochmann and Wilkinson,[35] we here report the synthesis of a vanadium-adamantyl complex, mononuclear $[V(OAd)_4]$ (^-OAd = 1-adamantoxide, complex **1**), by a different route with respect to that previously described. To the best of our knowledge, **1** represents the first homoleptic, "bare" V^{IV} alkoxide confirmed to be mononuclear and nearly tetrahedral, at room or higher temperature, by single-crystal X-ray diffraction analysis.

Additionally, given the emerging interest in a rational chemical design of highly coherent molecular spin centres for quantum information technology, and considering that no study has yet been reported on potential molecular qubits with low metal coordination numbers, we have also characterized the electronic properties of this singular $[V(OR)_4]$ complex through electron paramagnetic resonance (EPR) spectroscopy, and investigated its magnetization dynamics by alternate current (AC) susceptometry. The present report opens the way for the preparation of similar vanadium(IV) alkoxides in the solid state, to get better insights on their electronic structure, magnetic features and potential applications.

RESULTS AND DISCUSSION

Design and Synthesis. Bochmann and co-workers described the synthesis of a number of adamantyl-containing metal alkoxides, starting mainly from dialkylamide precursors. The 1-adamantoxide ligand was reported to form a mononuclear homoleptic complex with the "bare" vanadium(IV) cation,[35] but no crystal structure analysis was described for this product. The only reported compound characterised by the authors by X-ray crystallography was a heteroleptic molybdenum(IV) complex.

Whereas other tertiary alkoxides, such as tert-butoxide and tert-pentoxide, are known to form mononuclear products with non-oxido vanadium(IV) that are liquid at room temperature,[34,36] the 1-adamantoxide ligand gives a crystalline blue solid.[35] This alone

makes this complex interesting for detailed studies of the simple tetracoordinate vanadium(IV) unit through techniques that cannot be employed with liquid products. Moreover, the resistance against hydrolysis and oxidation offered by the bulky adamantyl group is a desirable quality in alkoxidovanadium complexes, most of which readily decompose if handled without utmost care in strict moisture- and air-exclusion conditions. Complex **1** is indeed remarkably resistant – after grinding to a fine powder and direct exposure to the air for up to six hours, no changes in the characteristic vibrational (FTIR) spectrum of the solid were observed, apart from moisture incorporation without any evidence of product hydrolysis (Figure S1). In the FTIR spectrum of **1** the most diagnostic absorptions have been attributed to the characteristic ν(C–O) vibration of alkoxides at 1101, 1070, 978 and 945 cm^{-1}, and to ν(V–O) at 689, 640, and 501 cm^{-1}.[37,38] These assignments have been discussed earlier.[35] The absence of an additional, strong absorption band related to the stretching mode of the V=O moiety at *ca* 1000 cm^{-1}, which is usually observed in oxidovanadium(IV) complexes,[39,40] supports the formation of a "bare" vanadium(IV) species as confirmed by single crystal X-ray diffraction analysis (vide infra).

In the present work, the [V(OAd)$_4$] complex was synthesised in high yield by alcoholysis of [V(OBu^t)$_4$] (a liquid starting material) with 1-adamantanol (a solid alcohol) in solution. In principle, although both tertiary alcohols in equation 1 present similarly small Brönsted acidity constants, the very low solubility of [V(OAd)$_4$] in organic solvents has probably functioned as the thermodynamic driving force to favour the direct reaction:

$$[V(OBu^t)_4] + 4\ HOAd \rightleftharpoons [V(OAd)_4] + 4\ HOBu^t \qquad [1]$$

Few other examples exist in the literature of structurally characterised adamantoxide-containing metal complexes, all of them heteroleptic.[18,41,42] In the case of the synthesis reported here, the reaction was conducted aiming for a homoleptic product, with the low radius of vanadium(IV) and steric hindrance of 1-adamantoxide precluding the additional coordination of *tert*-butanol, excess 1-adamantanol or solvent molecules.

Single-crystal X-ray diffraction analysis

A high degree of crystallographic disorder was observed during the refinement of the X-ray structure of product **1**. It involves the inner atoms, particularly the oxygen donor

atoms of the 1-adamantoxido ligands and some of the carbon atoms adjacent to these oxygen centres. This peculiar disorder, located very close to the vanadium centres and multiplied by the high number of symmetry operations of the cubic crystal system, brought a major degree of difficulty into the definition of the metal coordination sphere and the structure resolution as a whole.

Compound **1** crystallizes in the cubic $P\bar{4}3n$ space group with two crystallographically independent molecules in the asymmetric unit (selected dimensions in Table 1). In the molecule containing V(1) (Figure 1), the vanadium(IV) centre lies on a point of *23* (or *T*) symmetry; there are two of these molecules in the unit cell. The other molecule, of V(2) (Figure S2, Electronic Supplementary Information), has *-4* (or S_4) site symmetry; there are six of these in the cell. The S_4 symmetry is the same described by Haaland[43] for the liquid alkoxide [V(OBu^t)$_4$], Bu^t = *tert*-butyl, whose thermal average molecular structure was determined by gas-phase electron diffraction analysis. A packing diagram of the complex crystal structure of product **1** is shown in Figure S3. The molecules of V(1) occupy the vertices and the centre of the cubic cell, while the V(2) molecules arrange themselves in pairs on each face.
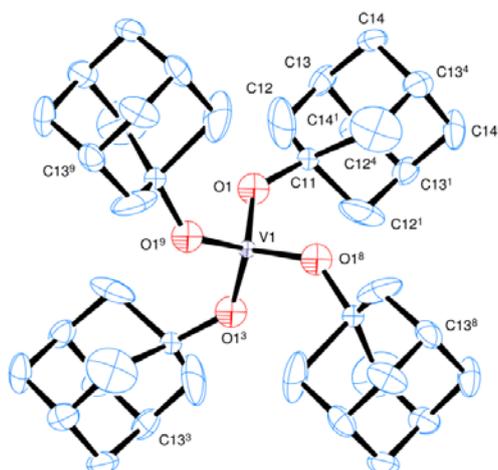

Figure 1 – View of the molecule of V(1) in **1**, indicating the atom numbering scheme; in each O-C group, only one of the three arrangements about a threefold symmetry axis (Figure S4) is displayed. Hydrogen atoms have been omitted for clarity. Thermal ellipsoids are drawn at the 30% probability level.

Table 1 – Selected molecular dimensions about the metal atoms in **1**. Bond lengths are in Ångstroms; angles in degrees. E.s.ds are in parentheses.

Molecule of V(1)			
V(1)-O(1)	1.794(18)	O(1)-V(1)-O(1[1])	93.4(11)
O(1)-C(11)	1.48(3)	O(1)-V(1)-O(1[2])	119.79(9)
		O(1)-V(1)-O(1[3])	119.30(17)
		O(1)-V(1)-O(1[4])	88.0(11)
		C(11)-O(1)-V(1)	136.6(14)
Molecule of V(2)			
V(2)-O(2)	1.761(9)	O(2)-V(2)-O(2[5])	112.0(3)
V(2)-O(21)	1.73(2)	O(2)-V(2)-O(2[6])	104.5(6)
V(2)-O(22)	1.84(2)	C(21)-O(2)-V(2)	124.9(9)
O(2)-C(21)	1.508(14)	C(21)-O(21)-V(2)	117.4(16)
O(21)-C(21)	1.67(3)	C(21)-O(22)-V(2)	112.9(15)
O(22)-C(21)	1.64(3)		

Symmetry transformations used to generate equivalent atoms:
1 -x,-y,z   2 z,-x,-y   3 -z,x,-y
4 -x,y,-z   5 -x,½-y,z   6 -x,y,1-y

The oxygen atoms bound to V(1) are disordered and displaced from the crystallographic threefold symmetry axes, Figure S4. The carbon atoms, C(11), bound to these oxygen donors are similarly disordered/displaced (and have been refined isotropically) in three distinct sites. The remaining carbon atoms were refined anisotropically in single, resolved sites. In the molecule of V(2), in turn, the oxygen atoms are disordered in distinct sites with occupancy ratios of *ca.* 0.55:0.25:0.20 about pseudo-threefold symmetry axes, while all carbon atoms were refined anisotropically in fully occupied sites, Figure 2.

There is therefore a major occupancy component in the disordered sets of oxygen atoms bound to V(2), which is identified in the unit cell representation by the O(2) labels. These four symmetry-related O(2) atoms do form a good tetrahedral shape about V(2), but the minor occupancy O atoms in this molecule form less recognizable tetrahedra. On the other hand, in the molecule of V(1) we have to admit that, while the refined partial atom sites give the best refinement, we do not have the complete picture of the individual components in the disordered systems. Discussion of molecular dimensions will therefore be limited principally to those of the V(2)/O(2) component molecule.
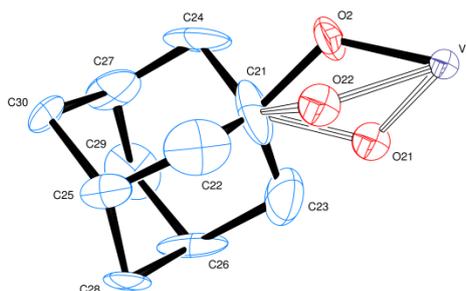
Figure 2 - A single V(2)–O–$C_{10}H_{15}$ unit showing the disorder in the O(2) atoms in the second crystallographically independent molecule of **1**. A diagram for the whole molecule containing V(2) is presented in Figure S2.

Bond distances are similar for the two crystallographically independent molecules of **1**. For the V(1) molecule, all V–O bond lengths are equivalent at 1.794(18) Å, while in the principal occupancy component of the V(2) molecule the bond lengths are equal to 1.761(9) Å (Table 1). These dimensions agree well with data for other vanadium(IV) alkoxides previously reported in the literature, both of the oxido- and non-oxido variety, which typically range between 1.7 and 1.9 Å for terminal alkoxido ligands.[20,22,34,44,45]

In the distorted tetrahedral V(2)/O(2) component of **1**, all the O-V-O angles are either 104.5(6) or 112.0(3)⁰ and the V-O-C angle is 124.9(9)⁰. V-O-C angles higher than the ideal tetrahedral (sp^3) figures are observed for alkoxide complexes with a significant π-donor contribution from the alkoxide to the metal-oxygen bond. For the tertiary alkoxide [V(OBuᵗ)₄],[43] for example, the corresponding bond angles are *ca* 138.6(18)⁰, larger than those found for the V(2) molecule of **1**, indicating a less significant π interaction between the metal ion and the bulkier adamantoxido ligand. For the homoleptic alkoxide series reported previously by our research group, the terminal RO⁻ ligands give V-O-C angles between 122 and 140⁰, with the isopropoxide and the bulkier neopentoxide providing the largest and smallest figures respectively.[34]

Structural data for **1** also display a satisfactory level of agreement with the only other mononuclear vanadium(IV) alkoxides crystallized to date, [V(OBuᵗ)₃{OSi(OBuᵗ)₃}] and [V(OBuᵗ)₂{OSi(OBuᵗ)₃}₂], both heteroleptic.[20] For the first molecule, which displays an unresolved site disorder between the similar silicon and vanadium(IV) centres, the bond lengths range from *ca* 1.68 to 1.73 Å. For the second compound, however, there is no such disorder and the V–O bond lengths are in excellent agreement with those recorded for product **1** (falling in the 1.76 to 1.78 Å range). Also, consistent with the presence of

tert-butoxide groups, the two V-O-C angles in this second reported product average at 134.4(2)°.

Spectroscopy studies by EPR

EPR spectroscopy data for **1** in the solid state (Figure 3) are compatible with a mononuclear species, displaying eight broad lines arising from the hyperfine coupling of the sole vanadium(IV) valence electron with its nucleus (I = 7/2). The observation of hyperfine splitting in this solid-state spectrum instead of a featureless broad line confirms the magnetically dilute nature of the unpaired spins in the sample, in which significant dipolar interactions among individual paramagnetic centres are probably reduced by the bulky nature of the 1-adamantyl group. This finds support in the fact that the shortest V···V distance in the unit cell is equal to 9.51 Å. The principal values for the ***g*** and ***A*** tensors, extracted from the simulation of the experimental spectrum, are shown in Figure 3 and compared in Table S1 with those recorded for other non-oxido mononuclear vanadium(IV) tetra-alkoxides.[34,46]

gx = 1.981
gy = 1.980
gz = 1.937
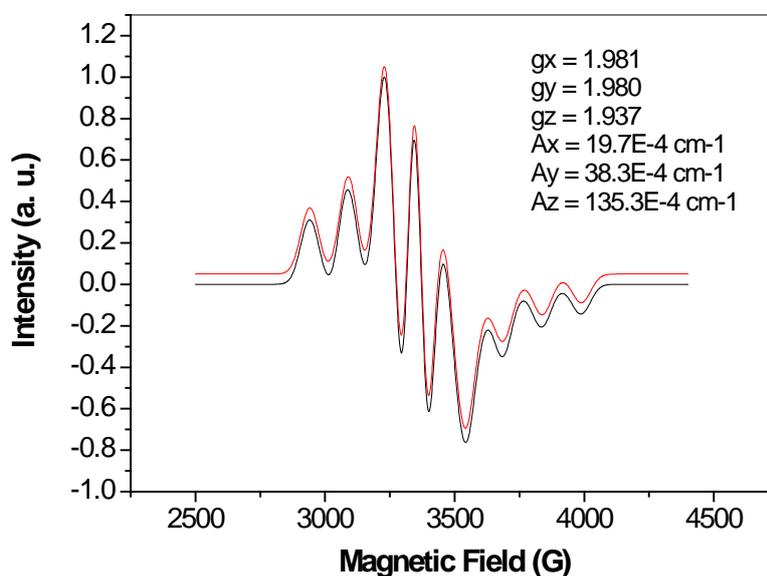Ax = 19.7E-4 cm-1
Ay = 38.3E-4 cm-1
Az = 135.3E-4 cm-1

Figure 3 – X-band EPR spectrum recorded at 77 K for the polycrystalline powder obtained by grinding the crystals of **1**. Black and red lines refer to the experimental and simulated spectra respectively.

Despite the large linewidth in the solid state spectrum of **1** in the bulk (Figure 3), it was possible to find a good fit for nearly axial g and A tensors, with relatively small differences between the perpendicular components (x and y). The more precisely determined z component (both for A and g) is clearly distinct from the perpendicular figures, and this evidences the axial character of the system. Based upon the refined X-ray data of **1** in which two types of crystallographically-independent molecules were identified, one could expect an isotropic signal coming from the molecules of V(1) – which occupy sites of average T-symmetry in the crystals – differently from the axial molecules of V(2). However, as the coordination environment around V(1) is highly disordered, it appears that for any individual molecule the actual symmetry is always lower than the crystal structure average, leading to the observation of the spectrum and parameters presented in Figure 3.

There is also a good correlation between the parameters found from the spectrum of **1** and those reported for other [V(OR)$_4$] complexes.[34,46] Once again, because of the paucity of EPR information on four-coordinate non-oxido V^{IV} compounds, it is still difficult to evaluate tendencies. Comparisons are possible with organometallic vanadium(IV) complexes such as [V(mes)$_4$][47] (mes = 2,4,6-trimethylbenzene) and [V(C$_6$Cl$_5$)$_4$][48], for which the same $g_z < g_x \approx g_y$ and relationship seen in Figure 3 holds. For these four-coordinate species, distortion of the tetrahedron by stretching (elongation) along the crystallographic c direction (taken as the z axis) decreases the point symmetry to D$_{2d}$ and C$_{2v}$ respectively.[47,48]

In the case of [V(mes)$_4$], for which a very elegant and complete single-crystal EPR study has been reported,[47] and in the more recent work on four-coordinate, Group 5 ketimide compounds published by Telser and Hayton[49] (D_{2d} symmetry), the low value of g$_z$, significantly smaller than the free-electron value of 2.0023, has been correlated with a d$_{x^2-y^2}^1$ electron configuration in the ground state.[50] As the point group symmetry decreases to C$_{2v}$ in [V(C$_6$Cl$_5$)$_4$], the ground state is reported to change from ^{2}B$_1$ (d$_{x^2-y^2}^1$ configuration) to ^{2}A$_2$ (d$_{xy}^1$).[48] In the case of complex **1**, the best defined V(2)/O(2) molecule occupies a site of S_4 symmetry and, according to X-ray data, is elongated along the c axis direction; this agrees with a ^{2}B (d$_{x^2-y^2}^1$) ground state assignment based on crystal field considerations for S_4 molecules.[51] However, the distinction between a d$_{xy}$ or a d$_{x^2-y^2}$ ground state cannot be made based on the available EPR parameters alone, requiring support from quantum-mechanical calculations. Recent work from Sanna *et al.*,[52] for example, presents DFT calculations of the hyperfine coupling tensor components ($A_{x,y,z}$)

for six-coordinate non-oxido vanadium(IV) complexes and, based on results, authors reach relevant conclusions about the impact of the single occupied molecular orbital (SOMO) composition on the values of the hyperfine tensor. For six-coordinate, "bare" V^{IV} species in which $A_z >> A_x \approx A_y$, with A_z varying between 135 and 155 × 10^{-4} cm^{-1}, compounds have been classified as "type 1" and correlated with a high percent contribution of the metal d_{xy} orbital to the SOMO. Such a relationship between the *A* component values is the same observed for complex **1** (Figure 3). As interesting and promising as these considerations are, it is not yet possible to draw correlations with the data obtained for **1** because of the different geometries and metal environments. Corresponding theoretical calculations for [V(OAd)$_4$] are under way in our group.

The spin Hamiltonian parameters determined for **1** (Figure 3) also find support in the EPR analysis of a dilute solid solution of [V(OAd)$_4$] in the diamagnetic [Ti(OAd)]$_4$ host (Figure 4 and Experimental section). The axial nature of the **g** and **A** tensors becomes evident in this environment. Although the synthesis of [Ti(OAd)]$_4$ had been described earlier,[35] its fully refined crystal structure had not been reported. We obtained single-crystal X-ray data for the V^{IV}-containing Ti^{IV} adamantoxide confirming both the same $P\bar{4}3n$ space group and structural features very similar to those reported here for [V(OAd)]$_4$ (Electronic Supplementary Material). Additionally, the symmetry of the spin-Hamiltonian tensor parameters derived for the doping V^{IV}, and the sharpness of the EPR lines in Figure 4 indicate that all vanadium centres in the solid solution occupy practically identical sites of axial symmetry, possibly the *-4* (*S$_4$*) sites in the cubic cell. This apparent segregation would be imposed by the more constraining, symmetric nature of the dispersing matrix composed of (d^0) titanium(IV) complexes as compared to bulk [V(OAd)]$_4$. This solid solution has been employed in pulsed-EPR experiments for the quantification of the quantum coherence time (*T$_m$*) for **1**, and thus investigate its potential usability as molecular qubit as compared with other vanadium(IV) complexes recently investigated in this respect.[53]
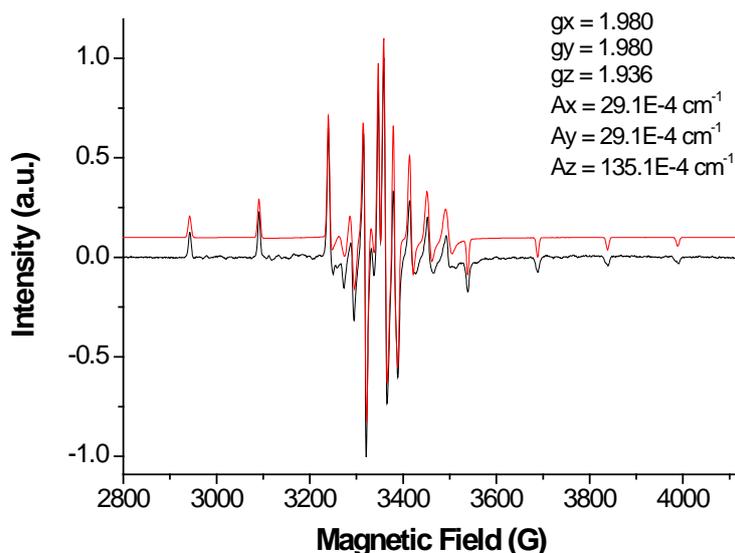
gx = 1.980
gy = 1.980
gz = 1.936
Ax = 29.1E-4 cm^{-1}
Ay = 29.1E-4 cm^{-1}
Az = 135.1E-4 cm^{-1}

Figure 4 – EPR spectrum recorded at 77 K for a solid solution of **1** (99.7:0.3 mol% Ti:V proportion) in a diamagnetic matrix of titanium(IV) adamantoxide, as described in the Experimental. The colourless crystals were ground to a fine powder before analysis. Black and red lines refer to the experimental and simulated spectrum respectively.

Magnetization dynamics. The magnetization dynamics of **1** has been investigated by AC susceptometry on polycrystalline samples. The thermal variation of the magnetic susceptibility in zero static magnetic field reveals no imaginary component of the susceptibility (χ'') in the whole investigated temperature range (3–30 K). When a small static magnetic field (> 0.040 T) is applied, slow magnetic relaxation is observed with appearance of a peak in the imaginary component of the susceptibility and a concomitant decrease of the real part (χ') (Figures S6–S10).

Under a static magnetic field of 1.0 T, **1** shows slow relaxation of the entire magnetization, so that this field was selected to investigate the temperature dependence of the spin-lattice relaxation time (τ). The frequency dependences of χ'' are satisfactorily reproduced with the Debye model (Figures S6) and the extracted values of τ as a function of the temperature are reported in Figure 5a.
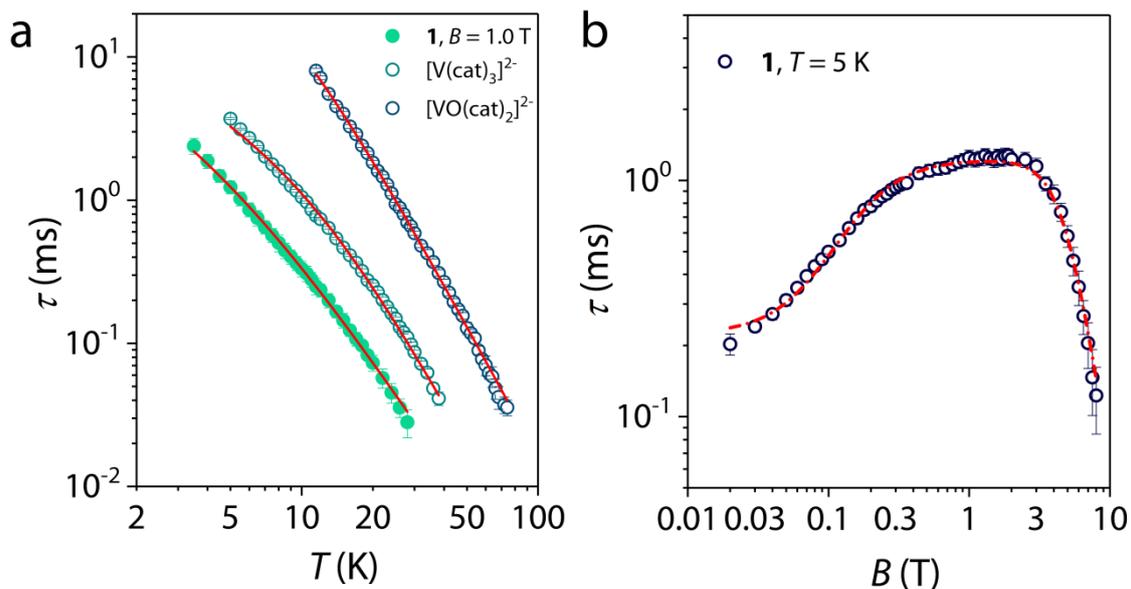
Figure 5 – (a) Temperature dependence of τ extracted from AC susceptibility measurements for a finely ground microcrystalline powder of compound **1** under an applied static magnetic field of 1.0 T. The graphic also shows a comparison with the temperature dependence of the spin-lattice relaxation times observed for finely ground square pyramidal oxidovanadium(IV) and octahedral non-oxido vanadium(IV) complexes with catecholate (cat) ligands, measured under the same conditions (B = 1.0 T).[53] (b) Magnetic field dependence of τ extracted from AC susceptibility measurements for compound **1** at T = 5 K (b). Continuous and dashed lines are for the best-fit models (see text).

Compound **1** shows slow magnetic relaxation up to *ca* 30 K (Figure S6) with relaxation times that range from *ca* 3 ms at 3 K to *ca* 0.02–0.03 ms at 30 K. The temperature dependence of τ, reported in Figure 5a as a *log*(τ) *vs log*(T) plot, shows a change in the slope as the temperature is increased above 10 K. This feature indicates a competition between the direct and the Raman mechanism of relaxation,[54] with the former and the latter dominating at temperatures lower and higher than 10 K, respectively.

To account for these two contributions to the relaxation, the spin-lattice relaxation rate, τ^{-1}, was fitted (solid lines in Figure 5) with the following model

$$\tau^{-1} = aT + bT^n \qquad [2]$$

where *a* is the coefficient of the direct mechanism, while *b* and *n* are the coefficient and the exponent of the Raman mechanism, respectively.[54] This model satisfactorily

reproduces the T dependence of τ with best-fit parameters: a = 75(8) μs^{-1} K^{-1}, b = 8.5(2) μs^{-1} K^{-n}, n = 2.5(1). The value of the Raman exponent n is particularly low with respect to what is expected for paramagnetic centres in inorganic solids (n = 7-9),[54] but commonly observed for vanadium(IV)-based molecular systems investigated through both AC susceptometry and pulsed EPR spectroscopy.[8,9,55] This also agrees with our earlier observations[56] about the inefficiency of the extended Raman term in the frame of the Debye model[57] to properly reproduce the spin-lattice relaxation data of these S = ½ molecular systems.

Analogous measurements performed on a microcrystalline but not finely ground sample of **1** (hereafter **1a**) shows slow relaxation on the magnetization (Figure S7) with longer relaxation times for T < 15 K, and comparable spin-lattice relaxation values for T > 15 K (Figure S8a). Such a behaviour is clearly ascribable to the spin-phonon bottleneck effect that dramatically enhances the spin-lattice relaxation times of vanadium(IV) S = ½ spin systems in the temperature range (typically T < 20 K) where the direct mechanism of relaxation dominates. The reason behind this effect is due to the inefficient transfer of heat from the crystal lattice to the thermal bath when crystallites assumes relevant dimensions.[58] Indeed, the difference in the slope of the $log(\tau)$ vs $log(T)$ plot for the finely ground sample **1** and the not finely ground microcrystalline sample **1a** (Figure S8) is in perfect agreement with what recently observed for some oxidovanadium(IV) complexes where this effect has been deeply investigated by controlling and varying the crystallite dimensions.[58]

In order to get better insights on the slow magnetic relaxation observed in Figure 5, the relaxation time was also investigated as a function of the static magnetic field in a wide field range (0.0−8.5 T). The relaxation times extracted with the Debye model (Figure S9) for **1** are reported in Figure 5b. The field dependence of the relaxation time shows a non-monotonous behaviour with an increase of τ as the strength of the static magnetic field increases, then it remains almost constant, and above 3.0 T starts to decrease.

This non-monotonous behaviour results from two effects occurring in different applied magnetic field regions. At low fields, spin-spin and spin-nuclei interactions promote rapid relaxation due to the mixing of the spin and nuclear magnetic states, while, at high fields, a higher phonon density matching the energy separation between the m_S = ±½ levels promotes a more efficient spin-phonon direct mechanism of relaxation ($\tau \propto B^4$). Thus, on increasing the field strength the suppression of the energy levels mixing allows for a

maximization of the relaxation time, while if the strength is increased further, the more efficient direct mechanism induces fast relaxation.

To account for these two contributions, the *B* dependence of the relaxation rate was reproduced with the Brons - van Vleck model[59,60]

$$\tau^{-1} = cB^4 + d\frac{1 + eB^2}{1 + fB^2} \qquad [3]$$

where the first term corresponds to the direct mechanism of relaxation, while the second takes into account the effect of an internal magnetic field in promoting relaxation, considered as a sum of spin-nuclei hyperfine and spin-spin dipolar interactions. The *B* dependence of τ for **1** is well reproduced through this model and the best-fit parameters are reported in Table S3. Measurements performed in the same conditions on **1a** (Figure S10) show a similar non-monotonous behaviour with longer relaxation times with respect to **1** for fields up 4.0 T, due to the predominant spin-phonon bottleneck regime occurring at the temperature selected for the measurements ($T = 5$ K). On the contrary, for $B > 4.0$ T, the spin-lattice relaxation times assumes comparable values (Figure S8b).

It is interesting to compare the thermal variation of the spin-lattice relaxation of **1** with those of pentacoordinate (square pyramidal) and hexacoordinate (trigonal prismatic) vanadium(IV) complexes recently investigated as potential molecular spin qubits.[53] Referring to the data that are not affected by spin-phonon bottleneck, it is worth noting that the relaxation times observed for this rare example of tetrahedrally-coordinate vanadium(IV) alkoxide are only slightly shorter than what recently reported for trigonal prismatic, tris-chelate complexes with catecholate ligands measured in analogous conditions (Figure 5a). This seems to correlate with the orbital contribution, which is smaller in the oxidovanadium system, as shown by the deviation of g_z from the free-electron value (1.956 for $[V(O)(cat)_2]^{2-}$, cat = catecholate,[53] *versus* 1.937 for **1**).

No striking differences in the slope of the curves are seen in Figure 5, but pulsed EPR experiments are required to investigate a wider temperature range, in which more pronounced differences have been observed between penta- and hexa-coordinated complexes.[55]

This result also confirms the remarkable properties of $S = 1/2$ vanadium(IV) complexes as slow relaxing spin systems, and their potential use as molecular spin qubits.[6,8,9,53,55,61,62]

CONCLUSIONS

Despite considerable difficulty imposed by both high symmetry and high crystallographic disorder, this work describes the crystallographic characterisation of the homoleptic and tetrahedral [V(OAd)$_4$], the only non-oxido vanadium(IV) alkoxide of its kind crystallized to date. The bulky ligand plays significant roles in protecting the "bare" V^{IV} cation from easy hydrolysis and oxidation, determining crystal packing and "diluting" the paramagnetic centres in the solid state, therefore minimising dipolar interactions and allowing the observation of hyperfine-split EPR spectra in the solid state.

This work adds new information into the study of non-oxido or "bare" vanadium(IV) complexes, particularly those of coordination numbers lower than six. Reports of this nature are still very scarce in the literature. EPR data obtained for **1**, together with data from previous reports,[47-49] indicate that the distorted tetrahedral environment of vanadium(IV) affects the nature of the electronic ground state and impacts directly on the magnitude of the A_z component of the hyperfine coupling tensor. These findings are in agreement with recent studies on six-coordinate non-oxido V^{IV} species, although expanded correlations involving different geometries depend on additional theoretical calculations.[52]

The spin dynamics is confirmed to be rather slow, comparable to other vanadium(IV) systems that can be coherently manipulated at room temperature.[9,55] An investigation by pulsed EPR spectroscopy could actually reveal appealing coherence times for this system. In fact, despite the high number of hydrogen atoms of the adamantane group, their reduced mobility has been considered at the origin of the best-performing coherence times observed in Cr$_7$Ni antiferromagnetic rings with bridging adamantanecarboxylate ligands.[63] The neutrality of the complex and the possibility to obtain an isostructural diamagnetic matrix using titanium(IV), also contribute to prompt further investigations on this material.

EXPERIMENTAL

General

All syntheses were carried out under strict inert atmosphere (N_2) conditions, employing standard Schlenk and glove-box techniques. All reagents were used as acquired from Aldrich, with the exception of titanium tetraisopropoxide (Merck), which was distilled under reduced pressure, and of 1-adamantanol, which was recrystallized at low temperature from a tetrahydrofuran (thf) solution previously kept over 4Å molecular sieves for a few days. Solvents (Aldrich) were treated by standard laboratory procedures and distilled under N_2 prior to use.[64] The vanadium starting materials [$VCl_3(thf)_3$][65] and [$V(OBu^t)_4$],[43] Bu^t = *tert*-butyl, were prepared *via* published methods.

Elemental analyses were performed by MEDAC Laboratories (Chobham, Surrey, UK). Carbon and hydrogen contents were determined by combustion analysis on a Thermal Scientific Flash EA 1112 Series Elemental Analyser. Metal (Ti and V) analyses were run by Inductively Coupled Plasma – Atomic Emission Spectroscopy (ICP-OES) with a Varian Vista MPX ICP-OES system. FTIR samples were analysed in Nujol mulls or KBr pellets using a BOMEM Hartmann & Braun spectrophotometer (MB series). EPR spectra were recorded on a Bruker EMX-Micro spectrometer at 300 and 77 K in the solid state, or in the toluene:thf mother liquor of **1** as mentioned in the text. Spectral simulations were performed with the EasySpin software[66] for the Matlab® platform; best-fit parameters were obtained with a *simplex* algorithm. The main directions of the **A** tensor were considered coincident with those for the gyromagnetic (**g**) tensor.

Syntheses

[V(OAd)$_4$], Ad = 1-adamantyl (product 1):

To a solution of [$V(OBu^t)_4$] (blue liquid, 0.51 g, 1.5 mmol) in 8 mL of toluene, a solution of 1-adamantanol (1.83 g, 12.0 mmol) in 10 mL of thf was slowly added. The royal blue reaction mixture then assumed a green-blue hue and was left standing at room temperature for 72 hours. After this period, the light blue product was filtered off and washed thoroughly with 40 mL of thf. The mother liquor was kept and analysed by EPR spectroscopy. Cooling this reaction mixture to -20°C led to crystallization of a second batch of blue crystals together with colourless crystals of 1-adamantanol; the latter were washed away with thf. Total yield of pure crystals of **1**, suitable for X-ray diffraction analysis: 0.63 g (63% for [$V(OAd)_4$]).

Found for **1**: 72.7% C; 9.06% H. Calc. for $C_{40}H_{60}O_4V$: 73.3% C; 9.22% H. FTIR (Nujol mull, Figure S1, with Nujol bands at 2923, 2852, 1451, 1377, 1349 and 721 cm^{-1}): 1310(w), 1296(m), 1282(w), 1264(vw), 1184(vw), 1179(vw), 1101(s) ν(C–O), 1070(vs) ν(C–O), 1034(w) ν(C–O), 978(vs) ν(C–O), 945(vs) ν(C–O), 931(m), 812(m), 794(s), 787(vs), 750(vs), 689(s) ν(M–O), 640(w) ν(M–O), 501(m) ν(M–O).

A solid solution of [V(OAd)$_4$] in [Ti(OAd)$_4$] was prepared by mixing liquid [Ti(OPr^i)$_4$] (146 mg, 0.513 mmol; Pr^i = isopropyl) with liquid [V(OBu^t)$_4$] (7.5 mg, 0.022 mmol) in 2.2 mL of toluene, followed by slow addition of a solution of 1-adamantanol (0.510 g, 3.35 mmol) in 2.7 mL of toluene. Colourless single crystals were formed after 24 h at room temperature and were shown to be isostructural with those of [V(OAd)$_4$] by X-ray crystallography. Found for the solid solution: 71.9% C; 9.11% H; 6.94% Ti; 0.02% V (99.7:0.3 mol% Ti:V proportion). Calc. for pure [Ti(OAd)$_4$], $C_{40}H_{60}O_4Ti$: 73.6% C; 9.26% H; 7.33% Ti.

Single-crystal X-ray diffraction analysis of product 1

Crystals of complex **1**, [V(OAd)$_4$], are clear, bright blue cubes that tend to form cracks after isolation from the mother liquor. From a sample under oil, one was mounted on a glass fibre and fixed in the cold nitrogen stream on an Oxford Diffraction Xcalibur Atlas Gemini Ultra diffractometer (at the Federal University of Minas Gerais, Brazil), equipped with Mo-Kα radiation, Atlas CCD area detector and graphite monochromator.

Data were processed using the CrysAlisPro-CCD and -RED programs (Oxford Diffraction, 2010). The structure was determined by the direct method routines in the space group P1 in the SHELXS program;[67-69] symmetry elements for the space group $P\bar{4}3n$ were added later. Refinement by full-matrix least-squares methods, on F^2's, was performed in SHELXL.[70] Although the collected X-ray data were sub-optimal due to weak diffraction at high angles and slight crystal degradation previous to measurement, the structure of **1** was confirmed as a mononuclear vanadium(IV) complex containing four 1-adamantoxide ligands. There are two independent molecules in this crystal; one lies with the vanadium atom on a point of *-4* symmetry, while the other molecule has *23* symmetry. The vanadium and carbon atoms of the adamantyl groups were mostly well defined and were refined anisotropically; the oxygen atoms were disordered and some of these were refined isotropically. Hydrogen atoms were included in idealised positions and their U$_{iso}$ values were set to ride on the U$_{eq}$ values of the parent carbon atoms.

The Flack indicator, x, at 0.48(13), suggested that the structure results were not complete. Different twinning patterns were then considered, and the Flack parameter for merohedral twinning was reduced to 0.05(4), but there were no significant changes in the R-factors and the e.s.ds of all refined parameters were greatly increased. The data reported here are for the single crystal with no twinning involved. Crystal data and final structure refinement details are presented in Table 3.

There appears to be residual electron density in the 'holes' between adamantyl groups in the crystal; partial occupation of these symmetry centres by oxygen atoms O(91) and O(92) was included in the final cycles of refinement.

Table 3 – Crystal data and structure refinement details for [V(OAd)$_4$], complex **1**

Elemental formula	C40 H60 O4 V
Formula weight	655.82
Crystal system, space group	Cubic, *P*-43*n* (no. 218)
Unit cell dimensions	$a = b = c$ = 19.0321(5) Å
	$\alpha = \beta = \gamma = 90°$
Volume	6893.8(3) Å^3
Z / calculated density	8 / 1.264 Mg/m^3
F(000)	2840
Absorption coefficient	0.328 mm^{-1}
Temperature	150.00(14) K
Wavelength	0.7107 Å
Crystal colour, shape	Bright blue, cubic blocks
Theta range for data collection	3.71 to 22.50°
Limiting indices	-18≤h≤20, -18≤k≤20, -20≤l≤20
Completeness to theta = 22.50	99.3%
Absorption correction	Semi-empirical from equivalents
Max. and min. transmission	1.00000 and 0.36961
Reflections collected (not including absences)	41128
No. of unique reflections	1510 [R(int) for equivalents = 0.163]
No. of 'observed' reflections (I > 2σ$_I$)	1071
Data / restraints / parameters	1510 / 0 / 149
Goodness-of-fit on F^2	1.104
Final R indices ('observed' data)	R_1 = 0.096, wR_2 = 0.238
Final R indices (all data)	R_1 = 0.125, wR_2 = 0.258

Absolute structure parameter	0.48(13)
Largest difference peak and hole	0.48 and -0.46 e/Å^3
Location of largest difference peak	near H(25)

Reflections weighted: w = $[\sigma^2(Fo^2)+(0.1619P)^2+1.601P]^{-1}$ where P=$(Fo^2+2Fc^2)/3$[70]

The crystal structure of complex **1** has also been independently solved at 100 K from a batch of crystals obtained from another preparation (same synthetic route described above). The structural data have also been deposited with the Cambridge Crystallographic Data Centre (CCDC _____, Supplementary Information). This second analysis provided a more complete set of data and has confirmed all structural features here described for **1**.

Single-crystal X-ray diffraction analysis of V-doped [Ti(OAd)$_4$]

Magnetic Measurements

AC susceptibility measurements were performed in the temperature range of 3.0−30 K with applied magnetic fields up to 8.5 T on polycrystalline samples of compounds **1** (40.2 mg) and **1a** (34.6 mg) by using a *Quantum Design Physical Property Measurement System (PPMS)* equipped with a AC susceptometer operating in the frequency range from 10 Hz to 10 kHz. Susceptibility data were corrected for the diamagnetic contributions as deduced by using Pascal's constant tables.[71]

ACKNOWLEDGEMENTS

collection for product **1**. D.S., D.L.H. and J.F.S. also thank CAPES and CNPq for fellowships.

SUPPLEMENTARY INFORMATION

FTIR spectra, additional ORTEP diagrams for complex **1**, solution EPR spectra (room temperature and 77 K) and magnetic data are presented as electronic supplementary information. CCDC reference numbers: 1835242.

REFERENCES

(1) Mandal, M.; Nagaraju, V.; Karunakar, G. V.; Sarma, B.; Borah, B. J.; Bania, K. K. Electronic, Conjugation, and Confinement Effects on Structure, Redox, and Catalytic Behavior of Oxido-Vanadium(IV) and -(V) Chiral Schiff Base Complexes. *The Journal of Physical Chemistry C* **2015**, *119*, 28854-28870.

(2) Cecchini, M. M.; De Angelis, F.; Iacobucci, C.; Reale, S.; Crucianelli, M. Mild catalytic oxidations of unsaturated fatty acid methyl esters (FAMEs) by oxovanadium complexes. *Applied Catalysis A: General* **2016**, *517*, 120-128.

(3) Hanson, S. K.; Baker, R. T. Knocking on Wood: Base Metal Complexes as Catalysts for Selective Oxidation of Lignin Models and Extracts. *Acc. Chem. Res.* **2015**, *48*, 2037-2048.

(4) Galloni, P.; Conte, V.; Floris, B. A journey into the electrochemistry of vanadium compounds. *Coord. Chem. Rev.* **2015**, *301-302*, 240-299.

(5) Smith, T. S.; LoBrutto, R.; Pecoraro, V. L. Paramagnetic spectroscopy of vanadyl complexes and its applications to biological systems. *Coord. Chem. Rev.* **2002**, *228*, 1-18.

(6) Zadrozny, J. M.; Niklas, J.; Poluektov, O. G.; Freedman, D. E. Millisecond Coherence Time in a Tunable Molecular Electronic Spin Qubit. *Acs Central Science* **2015**, *1*, 488-492.

(7) Bader, K.; Winkler, M.; van Slageren, J. Tuning of molecular qubits: very long coherence and spin-lattice relaxation times. *Chem. Commun.* **2016**, *52*, 3623-3626.

(8) Tesi, L.; Lucaccini, E.; Cimatti, I.; Perfetti, M.; Mannini, M.; Atzori, M.; Morra, E.; Chiesa, M.; Caneschi, A.; Sorace, L.; Sessoli, R. Quantum coherence in a processable vanadyl complex: new tools for the search of molecular spin qubits. *Chem. Sci.* **2016**, *7*, 2074-2083.

(9) Atzori, M.; Tesi, L.; Morra, E.; Chiesa, M.; Sorace, L.; Sessoli, R. Room-Temperature Quantum Coherence and Rabi Oscillations in Vanadyl Phthalocyanine: Toward Multifunctional Molecular Spin Qubits. *J. Am. Chem. Soc.* **2016**, *138*, 2154-2157.

(10) Yu, C. J.; Graham, M. J.; Zadrozny, J. M.; Niklas, J.; Krzyaniak, M. D.; Wasielewski, M. R.; Poluektov, O. G.; Freedman, D. E. Long Coherence Times

in Nuclear Spin-Free Vanadyl Qubits. *J. Am. Chem. Soc.* **2016**, *138*, 14678-14685.

(11) Graham, M. J.; Krzyaniak, M. D.; Wasielewski, M. R.; Freedman, D. E. Probing Nuclear Spin Effects on Electronic Spin Coherence via EPR Measurements of Vanadium(IV) Complexes. *Inorg. Chem.* **2017**, *56*, 8106-8113.

(12) Morgenstern, B.; Steinhauser, S.; Hegetschweiler, K.; Garribba, E.; Micera, G.; Sanna, D.; Nagy, L. Complex formation of vanadium(IV) with 1,3,5-triamino-1,3,5-trideoxy-cis-inositol and related ligands. *Inorg. Chem.* **2004**, *43*, 3116-3126.

(13) Dash, S. P.; Pasayat, S.; Bhakat, S.; Roy, S.; Dinda, R.; Tiekink, E. R. T.; Mukhopadhyay, S.; Bhutia, S. K.; Hardikar, M. R.; Joshi, B. N.; Patil, Y. P.; Nethaji, M. Highly Stable Hexacoordinated Nonoxidovanadium(IV) Complexes of Sterically Constrained Ligands: Syntheses, Structure, and Study of Antiproliferative and Insulin Mimetic Activity. *Inorg. Chem.* **2013**, *52*, 14096-14107.

(14) Kundu, S.; Mondal, D.; Bhattacharya, K.; Endo, A.; Sanna, D.; Garribba, E.; Chaudhury, M. Nonoxido Vanadium(IV) Compounds Involving Dithiocarbazate-Based Tridentate ONS Ligands: Synthesis, Electronic and Molecular Structure, Spectroscopic and Redox Properties. *Inorg. Chem.* **2015**, *54*, 6203-6215.

(15) Kajiwara, T.; Wagner, R.; Bill, E.; Weyhermuller, T.; Chaudhuri, P. Non-oxo 5-coordinate and 6-coordinate vanadium(iv) complexes with their precursor [LVIII(CH3OH)]0, where L = a trianionic aminetris(phenolate)-[N,O,O,O] donor ligand: a magnetostructural and EPR study. *Dalton Trans.* **2011**, *40*, 12719-12726.

(16) Byrne, E. K.; Richeson, D. S.; Theopold, K. H. Tetrakis(1-norbornyl)cobalt, a low spin tetrahedral complex of a first row transition metal. *J. Chem. Soc., Chem. Commun.* **1986**, 1491-1492.

(17) Power, P. P. Some highlights from the development and use of bulky monodentate ligands. *J. Organomet. Chem.* **2004**, *689*, 3904-3919.

(18) DiFranco, S. A.; Maciulis, N. A.; Staples, R. J.; Batrice, R. J.; Odom, A. L. Evaluation of Donor and Steric Properties of Anionic Ligands on High Valent Transition Metals. *Inorg. Chem.* **2012**, *51*, 1187-1200.

(19) Livage, J. Optical and electrical properties of vanadium oxides synthesized from alkoxides. *Coord. Chem. Rev.* **1999**, *190*, 391-403.

(20) Fujdala, K. L.; Tilley, T. D. New Vanadium Tris(tert-butoxy)siloxy Complexes and Their Thermolytic Conversions to Vanadia−Silica Materials. *Chem. Mater.* **2002**, *14*, 1376-1384.

(21) Danks, A. E.; Hall, S. R.; Schnepp, Z. The evolution of 'sol-gel' chemistry as a technique for materials synthesis. *Materials Horizons* **2016**, *3*, 91-112.

(22) Graf, D.; Schläfer, J.; Garbe, S.; Klein, A.; Mathur, S. Interdependence of Structure, Morphology, and Phase Transitions in CVD Grown VO2 and V2O3 Nanostructures. *Chem. Mater.* **2017**, *29*, 5877-5885.

(23) Albaric, L.; Hovnanian, N.; Julbe, A.; Volle, G. Oxovanadium(V)-1-methoxy-2-propanoxide: synthesis and spectroscopic studies - a molecular precursor for a vanadium-magnesium oxide catalyst. *Polyhedron* **2001**, *20*, 2261-2268.

(24) Nunes, G. G.; Friedermann, G. R.; Herbst, M. H.; Barthem, R. B.; Vugman, N. V.; Barclay, J. E.; Evans, D. J.; Hitchcock, P. B.; Leigh, G. J.; Sa, E. L.; Soares, J. F. The first hetero-binuclear alkoxide of iron and vanadium: structural and spectroscopic features. *Inorg. Chem. Commun.* **2003**, *6*, 1278-1281.

(25) Reis, D. M.; Westrup, K. C. M.; Nunes, G. G.; Barison, A.; Ribeiro, R. R.; de Sa, E. L.; Hughes, D. L.; Soares, J. F. Vanadium-Lithium Alkoxides: Synthesis,

Structure, Spectroscopic Characterisation and Accidental Degradation of Silicone Grease. *J. Braz. Chem. Soc.* **2009**, *20*, 613-626.

(26) O'Hanlon, S.; Glynn, C.; O'Dwyer, C. Effect of Annealing on the Development of Fully Transparent Ternary V-O-Na-Si Mixed Metal Oxide Thin Films from Polymer-Assisted Dip-Coated V2O5. *Ecs Journal of Solid State Science and Technology* **2016**, *5*, R3100-R3106.

(27) Zavahir, S.; Xiao, Q.; Sarina, S.; Zhao, J.; Bottle, S.; Wellard, M.; Jia, J. F.; Jing, L. Q.; Huang, Y. M.; Blinco, J. P.; Wu, H. S.; Zhu, H. Y. Selective Oxidation of Aliphatic Alcohols using Molecular Oxygen at Ambient Temperature: Mixed-Valence Vanadium Oxide Photocatalysts. *Acs Catalysis* **2016**, *6*, 3580-3588.

(28) Nachtigall, O.; Spandl, J. Versatile Organic Chemistry on Vanadium-Based Multi-Electron Reservoirs. *Chemistry-a European Journal* **2018**, *24*, 2785-2789.

(29) Steffensmeier, E.; Nicholas, K. M. Oxidation-reductive coupling of alcohols catalyzed by oxo-vanadium complexes. *Chem. Commun.* **2018**, *54*, 790-793.

(30) Menezes, W. G.; Reis, D. M.; Oliveira, M. M.; Soares, J. F.; Zarbin, A. J. G. Vanadium oxide nanostructures derived from a novel vanadium(IV) alkoxide precursor. *Chem. Phys. Lett.* **2007**, *445*, 293-296.

(31) Menezes, W. G.; Reis, D. M.; Benedetti, T. M.; Oliveira, M. M.; Soares, J. F.; Torresi, R. M.; Zarbin, A. J. G. V2O5 nanoparticles obtained from a synthetic bariandite-like vanadium oxide: Synthesis, characterization and electrochemical behavior in an ionic liquid. *J. Colloid Interface Sci.* **2009**, *337*, 586-593.

(32) Benedetti, T. M.; Redston, E.; Menezes, W. G.; Reis, D. M.; Soares, J. F.; Zarbin, A. J. G.; Torresi, R. M. Lithium intercalation in nanostructured thin films of a mixed-valence layered vanadium oxide using an ionic liquid electrolyte. *J. Power Sources* **2013**, *224*, 72-79.

(33) Nunes, G. G.; Friedermann, G. R.; dos Santos, J. L. B.; Herbst, M. H.; Vugman, N. V.; Hitchcock, P. B.; Leigh, G. J.; Sa, E. L.; da Cunha, C. J.; Soares, J. F. The first thermochromic vanadium(IV) alkoxide system. *Inorg. Chem. Commun.* **2005**, *8*, 83-88.

(34) Westrup, K. C. M.; Gregorio, T.; Stinghen, D.; Reis, D. M.; Hitchcock, P. B.; Ribeiro, R. R.; Barison, A.; Back, D. F.; de Sa, E. L.; Nunes, G. G.; Soares, J. F. Non-oxo vanadium(IV) alkoxide chemistry: solid state structures, aggregation equilibria and thermochromic behaviour in solution. *Dalton Trans.* **2011**, *40*, 3198-3210.

(35) Bochmann, M.; Wilkinson, G.; Young, G. B.; Hursthouse, M. B.; Malik, K. M. A. Preparation and properties of 1-adamantoxides, 2-adamantoxides, and 1-adamantylmethoxides of Ti, V, Nb, Nb, Cr, Cr, Mo, Mn, Fe, and Co. The crystal and molecular structure of tetrakis(1-adamantoxo)dimethylaminemolybdenum(IV). *J. Chem. Soc., Dalton Trans.* **1980**, 901-910.

(36) Bradley, D. C.; Mehta, M. L. Alkoxides of vanadium(IV). *Canadian Journal of Chemistry-Revue Canadienne De Chimie* **1962**, *40*, 1183-1188.

(37) Turova, N. Y.; Turevskaya, E. P.; Kessler, V. G.; Yanovskaya, M. I. *The Chemistry of Metal Alkoxides*; Springer: New York, 2002.

(38) Bradley, D. C. *Metal alkoxides*; Academic Press: New York, 1978.

(39) Nakamoto, K. *Infrared and Raman Spectra of Inorganic and Coordination Compounds*; 5th ed.; Wiley-Interscience: New York, 1997.

(40) Baran, E. J. Review: Spectroscopic studies of oxovanadium coordination compounds. *J. Coord. Chem.* **2001**, *54*, 215-238.

(41) Spielmann, J.; Harder, S. Reduction of Ketones with Hydrocarbon-Soluble Calcium Hydride: Stoichiometric Reactions and Catalytic Hydrosilylation. *Eur. J. Inorg. Chem.* **2008**, *2008*, 1480-1486.

(42) Gyepes, R.; Varga, V.; Horáček, M.; Kubišta, J.; Pinkas, J.; Mach, K. Influence of the Ti−O−C Angle on the Oxygen-to-Titanium π-Donation in [Cp2*Ti(III)OR] Complexes. *Organometallics* **2010**, *29*, 3780-3789.

(43) Haaland, A.; Rypdal, K.; Volden, H. V.; Andersen, R. A. Molecular structures of titanium(IV) and vanadium(IV) amides and alkoxides. *Journal of the Chemical Society-Dalton Transactions* **1992**, 891-895.

(44) Chang, Y.; Chen, Q.; Khan, M. I.; Salta, J.; Zubieta, J. Coordination chemistry of the tetrametalate core, {M4O16}: syntheses from [V2O2Cl2{(OCH2)2C(R)(CH2OH)}2] and structures of the mixed-metal cluster [V2Mo2O8(OMe)2{(OCH2)3CR}2]2- and the reduced cluster [V4O4(H2O)2(SO4)2{(OCH2)3CR}2]2. *J. Chem. Soc., Chem. Commun.* **1993**, 1872-1874.

(45) Salta, J.; Zubieta, J. Oxovanadium alkoxide complexes. Syntheses and crystal structures of (Ph4P)2[(VO)2Cl4(OR)2] (R = −CH3, −CH2CH2Cl) and [(VO)2Cl2MeC(CH2OH) (CH2O)22]. *Inorg. Chim. Acta* **1997**, *257*, 83-88.

(46) Kokoszka, G. F.; Allen, H. C.; Gordon, G. The Electron Paramagnetic Resonance Spectrum of Tetrakis-t-butoxyvanadium(IV). *Inorg. Chem.* **1966**, *5*, 91-93.

(47) Kirmse, R.; Stach, J.; Kreisel, G. A single-crystal ESR study on a tetrahedrally coordinated vanadium(IV) compound: tetramesitylvanadium(IV). *J. Organomet. Chem.* **1981**, *210*, 73-82.

(48) Alonso, P. J.; Forniés, J.; García-Monforte, M. A.; Martín, A.; Menjón, B. New Homoleptic Organometallic Derivatives of Vanadium(III) and Vanadium(IV): Synthesis, Characterization, and Study of Their Electrochemical Behaviour. *Chem. - Eur. J.* **2005**, *11*, 4713-4724.

(49) Damon, P. L.; Liss, C. J.; Lewis, R. A.; Morochnik, S.; Szpunar, D. E.; Telser, J.; Hayton, T. W. Quantifying the Electron Donor and Acceptor Abilities of the Ketimide Ligands in M(N=CtBu2)4 (M = V, Nb, Ta). *Inorg. Chem.* **2015**, *54*, 10081-10095.

(50) Weil, J. A.; Bolton, J. R. *The Interpretation of EPR Parameters*. In *Electron Paramagnetic Resonance*; Weil, J. A., Bolton, J. R., Eds.; John Wiley & Sons: New York, 2006, p 253-300.

(51) Lever, A. B. P. *Inorganic Electronic Spectroscopy*; 2nd ed.; Elsevier: New York, 1984.

(52) Sanna, D.; Sciortino, G.; Ugone, V.; Micera, G.; Garribba, E. Nonoxido VIV Complexes: Prediction of the EPR Spectrum and Electronic Structure of Simple Coordination Compounds and Amavadin. *Inorg. Chem.* **2016**, *55*, 7373-7387.

(53) Atzori, M.; Benci, S.; Morra, E.; Tesi, L.; Chiesa, M.; Torre, R.; Sorace, L.; Sessoli, R. Structural Effects on the Spin Dynamics of Potential Molecular Qubits. *Inorg. Chem.* **2018**, *57*, 731-740.

(54) Standley, K. J.; Vaughan, R. A. *Electron Spin Relaxation Phenomena in Solids*; Plenum Press: New York, 1969.

(55) Atzori, M.; Morra, E.; Tesi, L.; Albino, A.; Chiesa, M.; Sorace, L.; Sessoli, R. Quantum Coherence Times Enhancement in Vanadium(IV)-based Potential Molecular Qubits: the Key Role of the Vanadyl Moiety. *J. Am. Chem. Soc.* **2016**, *138*, 11234-11244.

(56) Atzori, M.; Tesi, L.; Benci, S.; Lunghi, A.; Righini, R.; Taschin, A.; Torre, R.; Sorace, L.; Sessoli, R. Spin Dynamics and Low Energy Vibrations: Insights from Vanadyl-Based Potential Molecular Qubits. *J. Am. Chem. Soc.* **2017**, *139*, 4338-4341.

(57) Fielding, A. J.; Fox, S.; Millhauser, G. L.; Chattopadhyay, M.; Kroneck, P. M. H.; Fritz, G.; Eaton, G. R.; Eaton, S. S. Electron spin relaxation of copper(II) complexes in glassy solution between 10 and 120K. *Journal of Magnetic Resonance* **2006**, *179*, 92-104.

(58) Tesi, L.; Lunghi, A.; Atzori, M.; Lucaccini, E.; Sorace, L.; Totti, F.; Sessoli, R. Giant spin-phonon bottleneck effects in evaporable vanadyl-based molecules with long spin coherence. *Dalton Trans.* **2016**, *45*, 16635-16643.

(59) Van Vleck, J. H. Paramagnetic Relaxation Times for Titanium and Chrome Alum. *Physical Review* **1940**, *57*, 426-447.

(60) De Vroomen, A. C.; Lijphart, E. E.; Prins, D. Y. H.; Marks, J.; Poulis, N. J. Electron spin-lattice relaxation of the Zeeman and interaction systems in CuCs2(SO4)2·6H2O. *Physica* **1972**, *61*, 241-249.

(61) Zadrozny, J. M.; Niklas, J.; Poluektov, O. G.; Freedman, D. E. Multiple Quantum Coherences from Hyperfine Transitions in a Vanadium(IV) Complex. *J. Am. Chem. Soc.* **2014**, *136*, 15841-15844.

(62) Graham, M. J.; Zadrozny, J. M.; Fataftah, M. S.; Freedman, D. E. Forging Solid-State Qubit Design Principles in a Molecular Furnace. *Chem. Mater.* **2017**, *29*, 1885-1897.

(63) Wedge, C. J.; Timco, G. A.; Spielberg, E. T.; George, R. E.; Tuna, F.; Rigby, S.; McInnes, E. J. L.; Winpenny, R. E. P.; Blundell, S. J.; Ardavan, A. Chemical Engineering of Molecular Qubits. *Phys. Rev. Lett.* **2012**, *108*, 107204.

(64) Perrin, D. D.; Armarego, W. L. *Purification of Laboratory Chemicals*; 3rd ed.; Butterworth-Heinemann: Oxford, 1997.

(65) Manzer, L. E. Tetrahydrofuran complexes of selected early transition-metals. *Inorg. Synth.* **1982**, *21*, 135-140.

(66) Stoll, S.; Schweiger, A. EasySpin, a comprehensive software package for spectral simulation and analysis in EPR. *Journal of Magnetic Resonance* **2006**, *178*, 42-55.

(67) Sheldrick, G. A short history of SHELX. *Acta Crystallogr., Sect. A: Found. Adv.* **2008**, *64*, 112-122.

(68) Sheldrick, G. M. Crystal structure refinement with SHELXL. *Acta Crystallographica Section C-Structural Chemistry* **2015**, *71*, 3-8.

(69) Sheldrick, G. M., *SHELXS – Programs for crystal structure determination (SHELXS-2013)* (2013) University of Göttingen, Germany.

(70) Sheldrick, G. M., *SHELXL – Programs for crystal structure refinement (SHELXL-2014)*, (2014) University of Göttingen, Germany.

(71) Bain, G. A.; Berry, J. F. Diamagnetic Corrections and Pascal's Constants. *J. Chem. Educ.* **2008**, *85*, 532.

For Table of Contents only

TOC graphic and synopsis
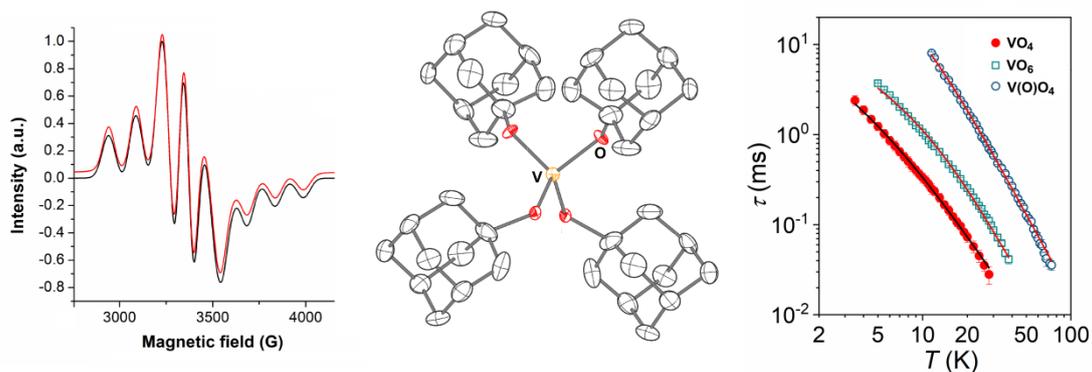
This work describes the crystallographic characterisation of the homoleptic and distorted tetrahedral [V(OAd)$_4$] (**1**), the only non-oxido vanadium(IV) alkoxide of its kind crystallized to date. Spin Hamiltonian parameters extracted from EPR spectra at 77 K ($g_z < g_x \approx g_y$ and $A_z >> A_x \approx A_y$) have been compared with literature data to provide insights into the electronic structure of **1**. Magnetization dynamics measurements by AC susceptometry revealed field-induced slow spin relaxation comparable to that of other vanadium(IV) potential molecular qubits.

Electronic Supplementary Information

A rare example of four-coordinate non-oxido vanadium(IV) alkoxide in the solid state: structure, spectroscopy and magnetization dynamics

Danilo Stinghen,[a] Matteo Atzori,[b] Caprici M. Fernandes,[a] Ronny R. Ribeiro,[a]
Eduardo L. de Sá,[a] Davi F. Back,[c] David L. Hughes,[d] Giovana G. Nunes,[a]
Mario Chiesa,[e] Renato Torre,[e] Roberta Sessoli[b] and Jaísa F. Soares[a,*]

[a]*Departamento de Química, Universidade Federal do Paraná, Centro Politécnico, Jardim das Américas, 81530-900 Curitiba-PR, Brazil*

[b] *Dipartimento di Chimica "Ugo Schiff" and INSTM RU, Università degli Studi di Firenze, Via della Lastruccia 3, 50019 Sesto Fiorentino (FI), Italia*

[c] *Departamento de Química, Universidade Federal de Santa Maria, Camobi, 97105-900 Santa Maria-RS, Brazil*

[d] *School of Chemistry, University of East Anglia, Norwich NR4 7TJ, UK*

[e] *Dipartimento di Chimica e NIS Centre, Università di Torino, Via P. Giuria 7, I10125 Torino, Italia*

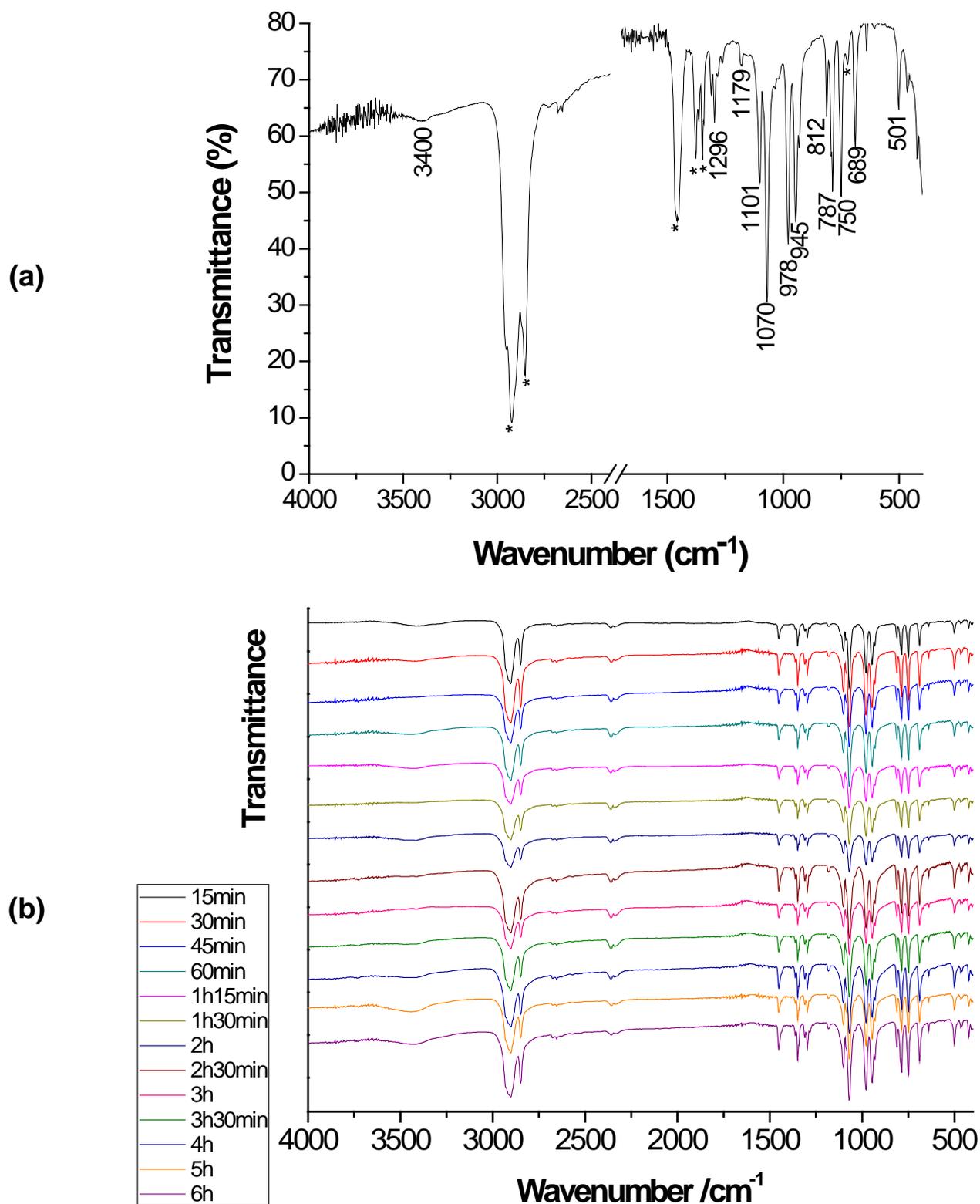*Correspondence to: J. F. Soares (e-mail: jaisa@quimica.ufpr.br)*

Figure S1 – FTIR spectra registered for complex **1** in Nujol mull under dry N_2 (a) and in KBr pellets after exposition to the air for up to 6 hours (b). In (a), bands marked with asterisks coincide with absorptions from Nujol. In (b), the increasing intensity of the absorption at *ca* 3400 cm^{-1} indicates incorporation of moisture, but there are no changes in the specific absorptions of **1** that could indicate hydrolysis.
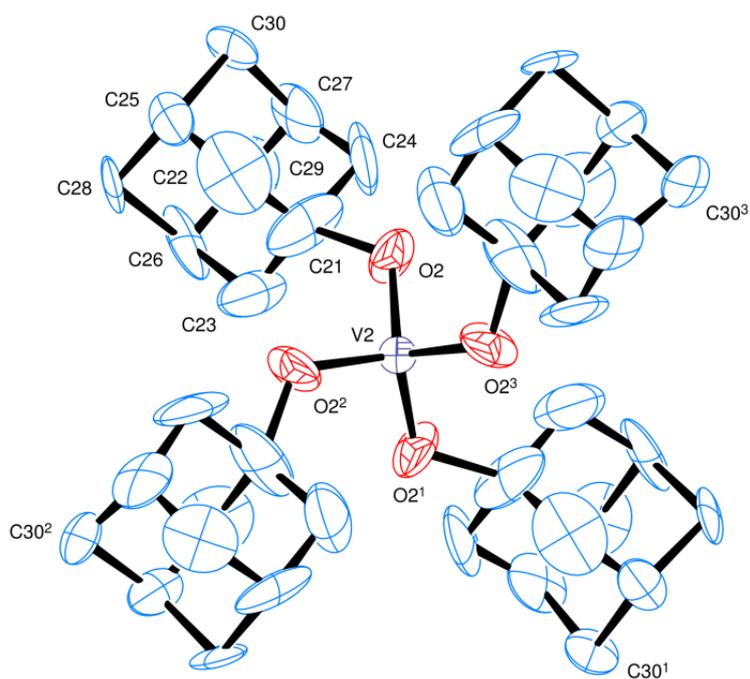
Figure S2 – Representation of the second (V2) crystallographically-independent molecule of [V(OAd)$_4$] (**1**), showing the principal components of the disordered oxygen atoms. This view corresponds to the one shown for the first molecule in Figure 2 (main text).
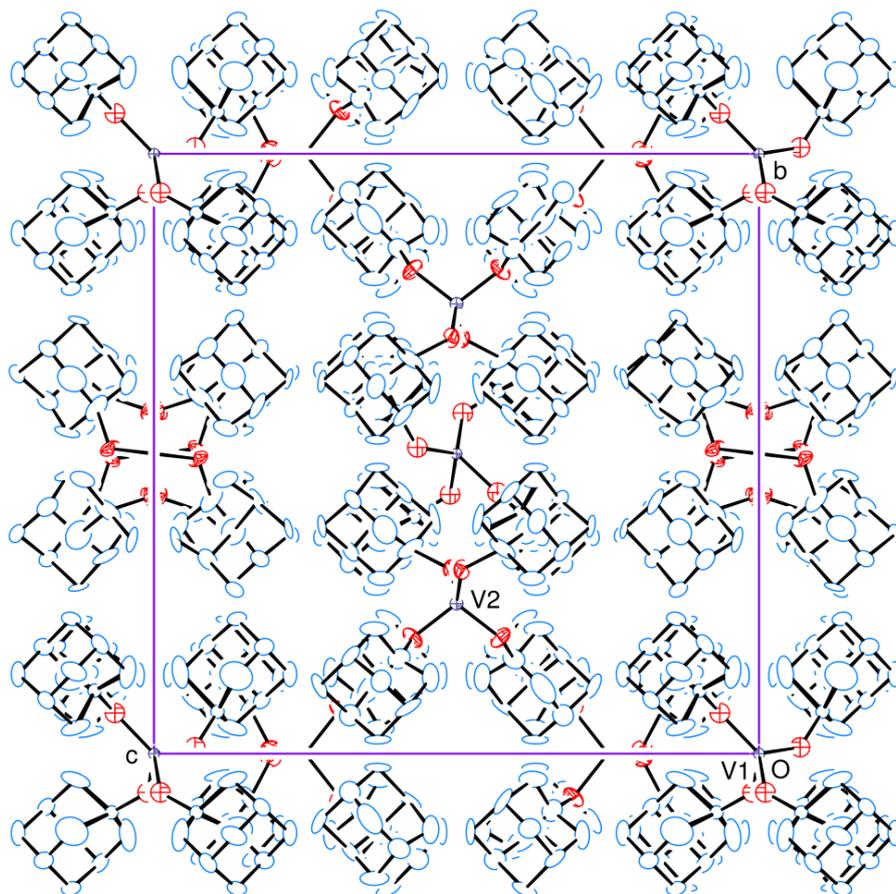
Figure S3 – View of the cell of [V(OAd)₄] down the *a* axis. The disordered VO₄ groups are displayed as in Figures 1 and S2. The sites of residual electron density, represented by atoms O(91) and O(92), are not shown.
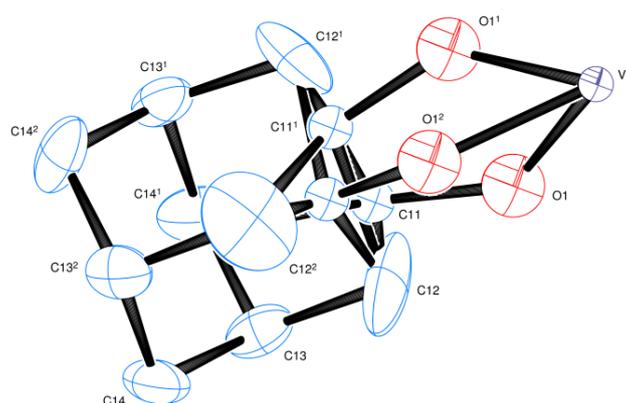

Figure S4 – A single V-O-C₁₀H₁₅ unit, showing the disorder in the O(1) and C(11) atoms in the first molecule of [V(OAd)₄]. A three-fold proper rotation axis passes through V(1) and relates the O(1), O(1¹) and O(1²) components of the disordered set of donor atoms.
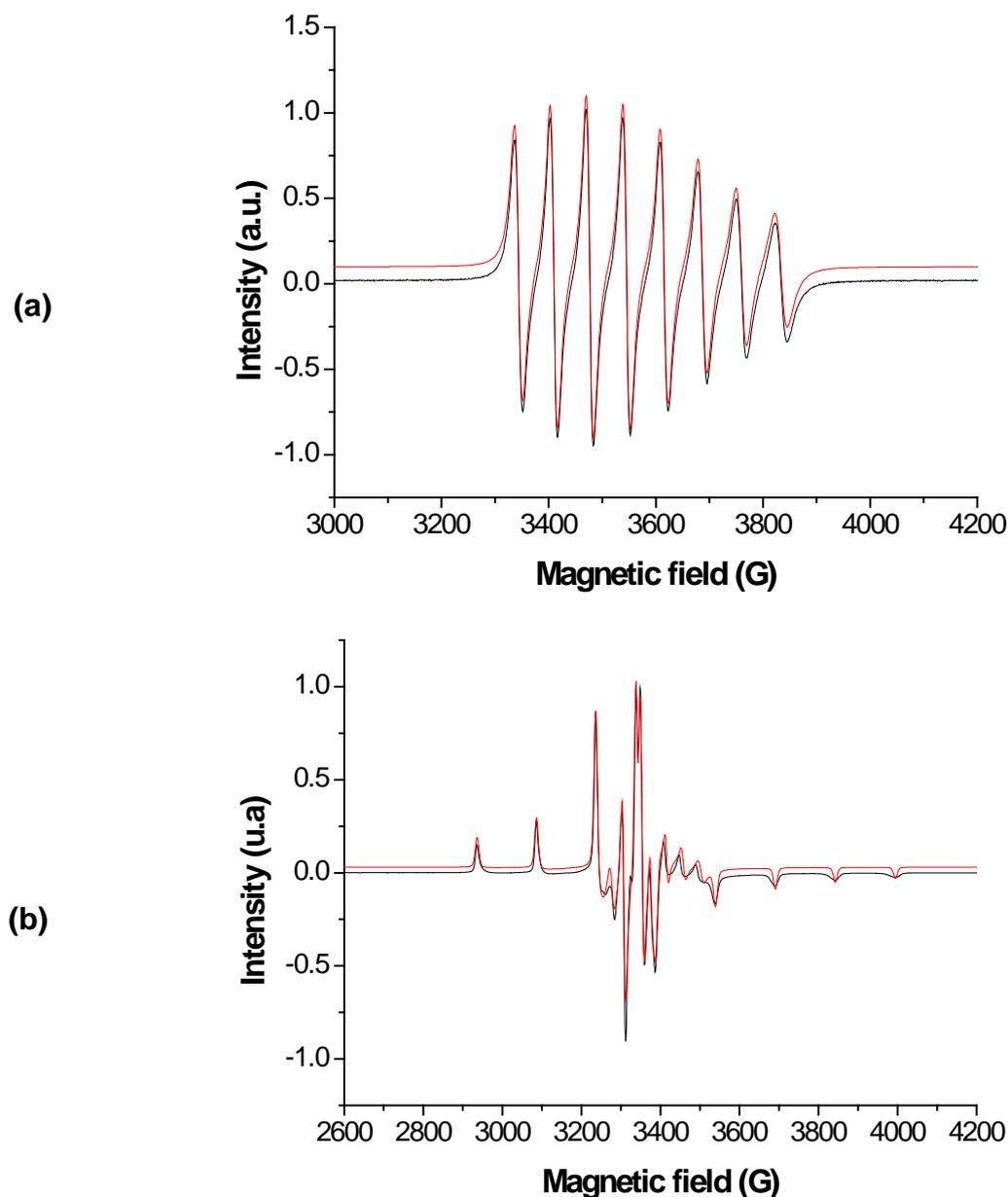
Figure S5 – EPR spectra recorded for the reaction mixture from which **1** was formed (thf/toluene mixture) at room temperature (a) and 77 K (frozen solution, b). Black lines comprise the experimental data, while the red lines are for the best simulations. Parameters are presented in Tables S1 and S2.

Complex **1** presents very low solubility in aprotic organic solvents; to circumvent this problem, the solution spectra reported in Figure S5 were registered directly from the mother liquor that produced crystals of **1**. All EPR parameters (Table S1) agree well with those from the solid-state spectrum (Figure 3) and from the spectrum of the solid solution of **1** in the isostructural $[Ti(OAd)_4]$ (Figure 4), but the similarity of these data with those recorded for solutions of $[V(OBu^t)_4]$ and $[V(OPe^t)_4]$ (also on Table S1) does not allow any clear distinction. Further studies were then carried out, as shown in Table S2 and discussed below.

Table S1 – EPR parameters obtained for **1**, in comparison with those of the liquid vanadium(IV) alkoxides [V(OBu^t)$_4$] and [V(OPe^t)$_4$]

Parameters	Complex 1[(a)]			[V(OBu^t)$_4$][34,46]		[V(OPe^t)$_4$][34]	
	Solid State[(b)]	Fluid or frozen solutions					
		RT[(c)]	77 K[(c)]	RT	77 K	RT	77 K
g$_x$	1.981	1.977	1.983	1.983	1.985	1.980	1.985
g$_y$	1.980	1.977	1.978	1.983	1.980	1.980	1.980
g$_z$	1.937	1.929	1.931	1.918	1.934	1.921	1.933
g$_{iso}$ or g$_{avg}$	1.966	1.962	1.964	1.962	1.966	1.961	1.966
A$_x$ (10^{-4} cm^{-1})	19.7	(d)	22.9	(d)	21.7	(d)	20.8
A$_y$ (10^{-4} cm^{-1})	38.3		32.4		31.5		31.6
A$_z$ (10^{-4} cm^{-1})	135.3		136.1		135.7		135.7
A$_{iso}$ (10^{-4} cm^{-1})	64.4	64.0	64.8	64.3	63.0	64.4	62.7

[V(OBu^t)$_4$] and [VO(Pe^t)$_4$] were analysed in toluene solution (10 mmol L^{-1}).
g$_{iso}$ is employed for room temperature studies, and g$_{avg}$ (average) for frozen solutions or solid state.
[a] Early report for **1** in diluted benzene solution at 295K: g$_{iso}$ = 1.9863, A$_{iso}$ = 64.9 10^{-4} cm^{-1}.[35]
[b] Spectrum recorded for the polycrystalline power obtained by grinding the crystals of **1**.
[c] Spectra recorded from the mother liquor (toluene/thf mixture, according to Experimental).
[d] Only A$_{iso}$ was obtained in these simulations.

The room-temperature solution data were simulated with fast-motional regime algorithms, which allowed us to calculate the mean rotational radius of the paramagnetic species in solution (Table S2). The value for complex **1** is much larger than those reported for [V(OBu^t)$_4$] and [V(OPe^t)$_4$], even taking into account the viscosity difference of the solvents in which the measurements were performed (toluene:thf 1:1.25 for **1** and pure toluene for the other compounds). The higher values of both correlation time and rotational radius presented by **1** agree well with the larger volume of the [V(OAd)$_4$] paramagnetic species, and support the full replacement of *tert*-butoxide with 1-adamantoxide during the synthesis of **1**.

Table S2 – Rotational dynamics of **1** in the mother liquor at room temperature, evaluated from the EPR spectra, in comparison with those of the liquid vanadium(IV) alkoxides [V(OBu^t)$_4$] and [V(OPe^t)$_4$]

Parameters	Rotational dynamics in solution at room temperature		
	Complex 1	[V(OBu^t)$_4$]	[V(OPe^t)$_4$]
Correlation time, τ$_c$ (10^{-12} s)	25.3	4.11	5.48
Rotational radius (10^{-10} m)	3.62	1.89	2.08

$$\chi''(\omega) = (\chi_T - \chi_S) \frac{(\omega\tau)^{1-\alpha} \cos\left(\frac{\pi\alpha}{2}\right)}{1 + 2(\omega\tau)^{1-\alpha} \sin\left(\frac{\pi\alpha}{2}\right) + (\omega\tau)^{2-2\alpha}}$$

Equation S1 – Equation of the Debye model used for the extrapolation of the relaxation times τ through AC susceptibility measurements. χ'' is the imaginary susceptibility, χ_T is the isothermal susceptibility, χ_S is the adiabatic susceptibility, ω is the angular frequency, and α is the distribution width of the relaxation time.
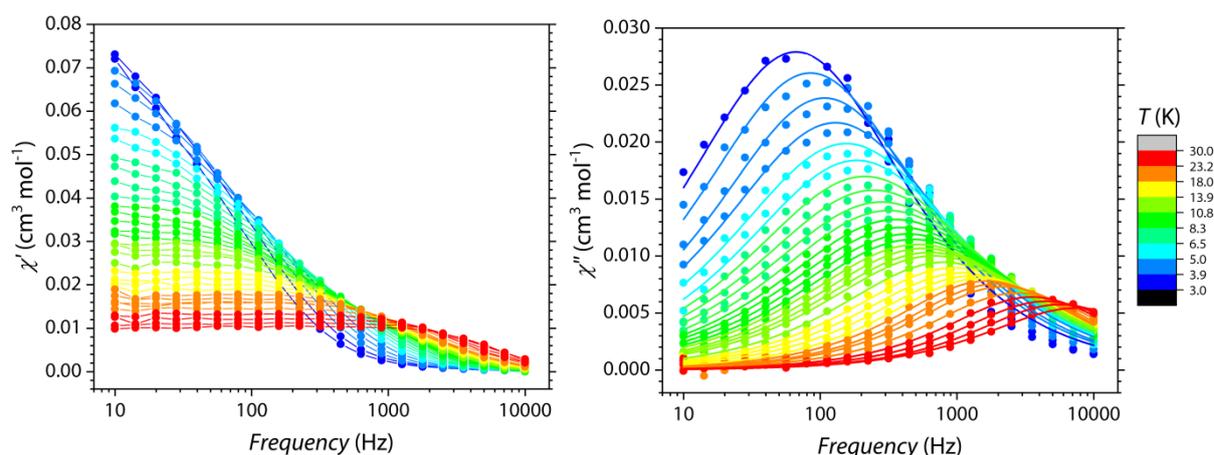
Figure S6 – Frequency dependence of the real component χ' (left) and the imaginary component χ'' (right) of the magnetic susceptibility of **1** as a function of the temperature (3.0–30 K range) under an applied static magnetic field of 1.0 T. For χ'', the continuous lines represent the best-fit to the Debye equation (Eq. S1).
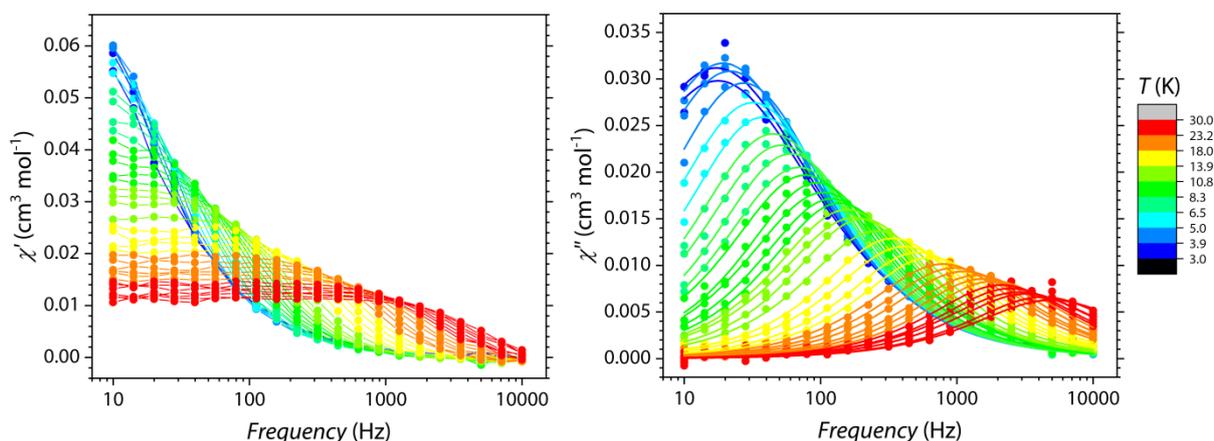

Figure S7 – Frequency dependence of the real component χ' (left) and the imaginary component χ'' (right) of the magnetic susceptibility of **1a** as a function of the temperature (3.0–30 K range) under an applied static magnetic field of 1.0 T. For χ'', the continuous lines represent the best-fit to the Debye equation (Eq. S1).
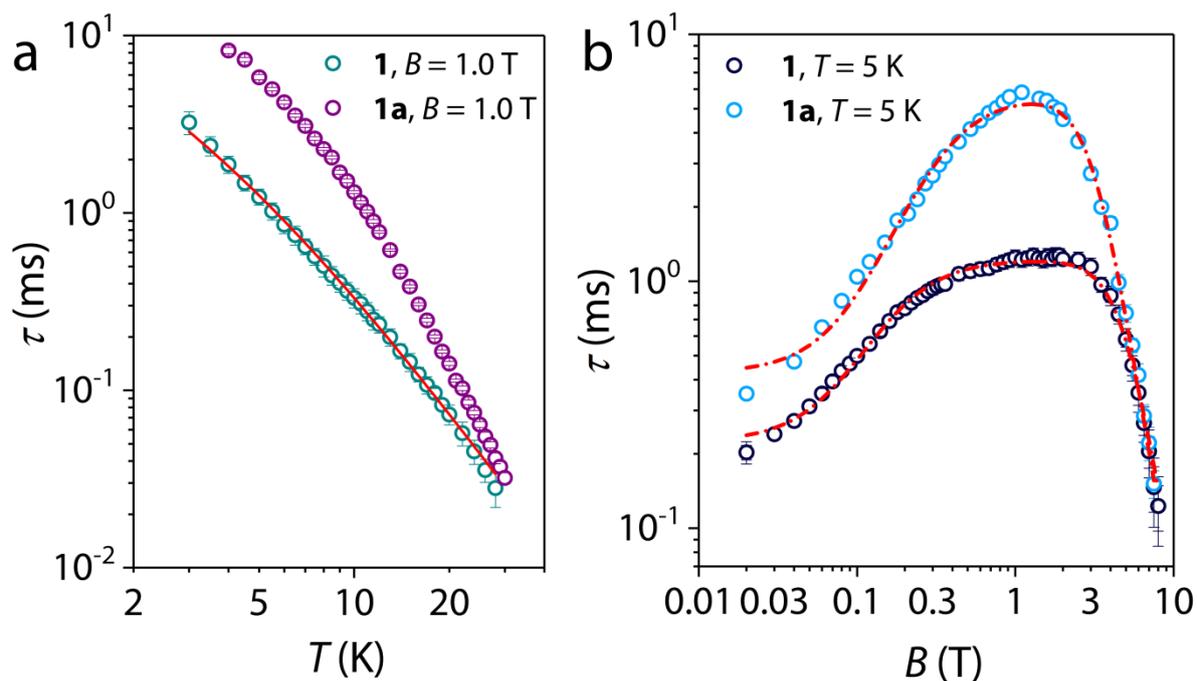
Figure S8 – Comparison between the thermal (a) and magnetic field (b) dependence of the spin-lattice relaxation time for **1** and **1a** measured in the same conditions (see legend).
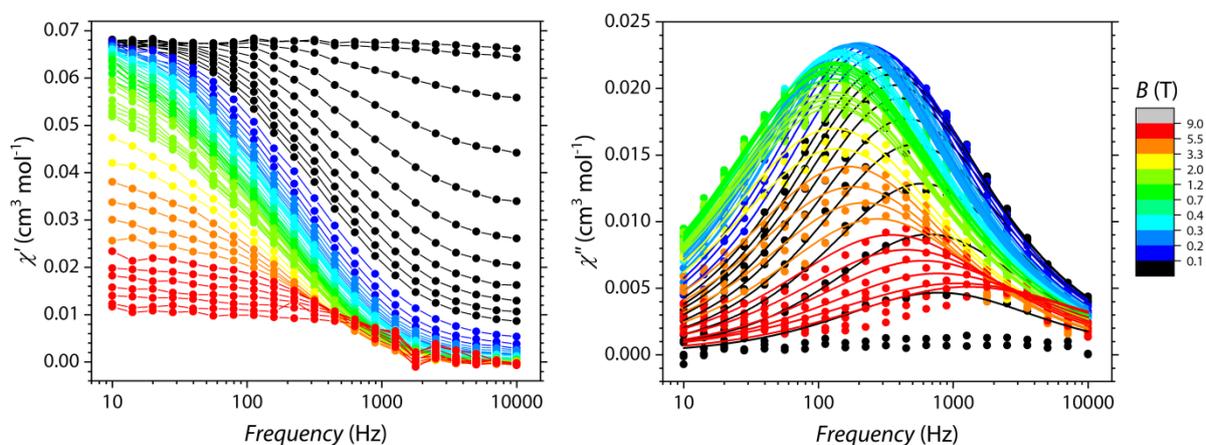

Figure S9 – Frequency dependence of the real component χ' (left) and the imaginary component χ'' (right) of the magnetic susceptibility of **1** as a function of the magnetic field (0.0–8.5 T range) at $T = 5$ K. For χ'', the continuous lines represent the best-fit to the Debye equation (Eq. S1).
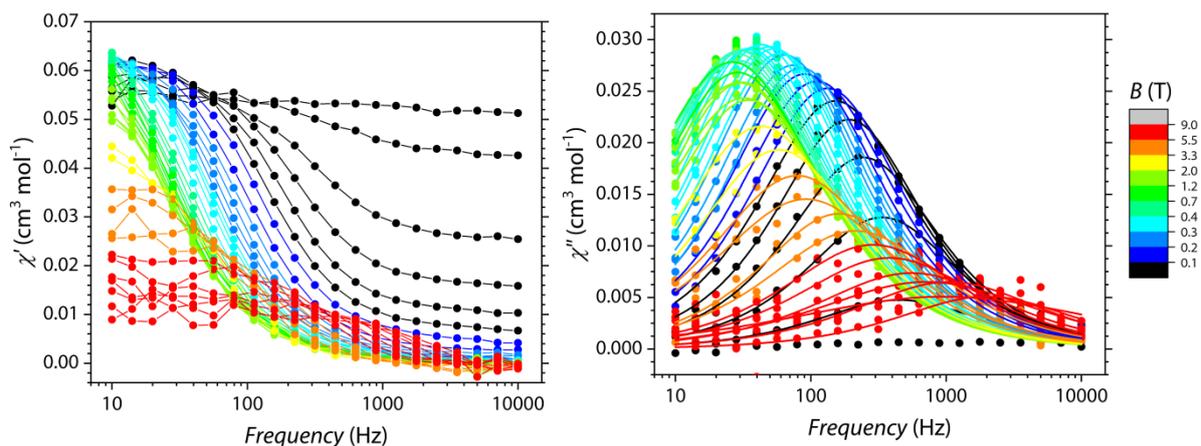
Figure S10 – Frequency dependence of the real component χ' (left) and the imaginary component χ'' (right) of the magnetic susceptibility of **1a** as a function of the magnetic field (0.0–8.5 T range) at T = 5 K. For χ'', the continuous lines represent the best-fit to the Debye equation (Eq. S1).

Table S3 – Best-fit parameters of the model used to reproduce the field dependence of the magnetization relaxation rate for **1** and **1a** at T = 5 K

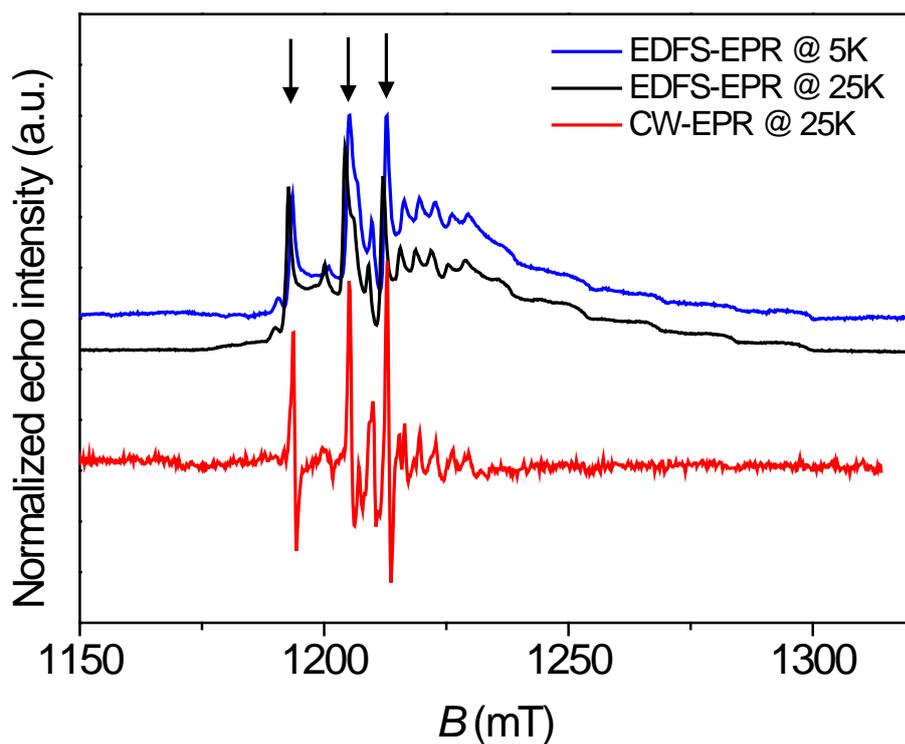| Compound	c (T^{-4}μs^{-1})	d (ms^{-1})	e (T^{-2})	f (T^{-2})
1	2.0(1)	2.3(1)	9.7(7)	129(10)
1a	1.5(1)	4.5(1)	34(2)	188(13)

Figure Sx Q-band CW and ESE EPR spectra recorded at different temperatures as indicated. The arrows indicate the observer positions where the ENDOR spectra have been recorded.
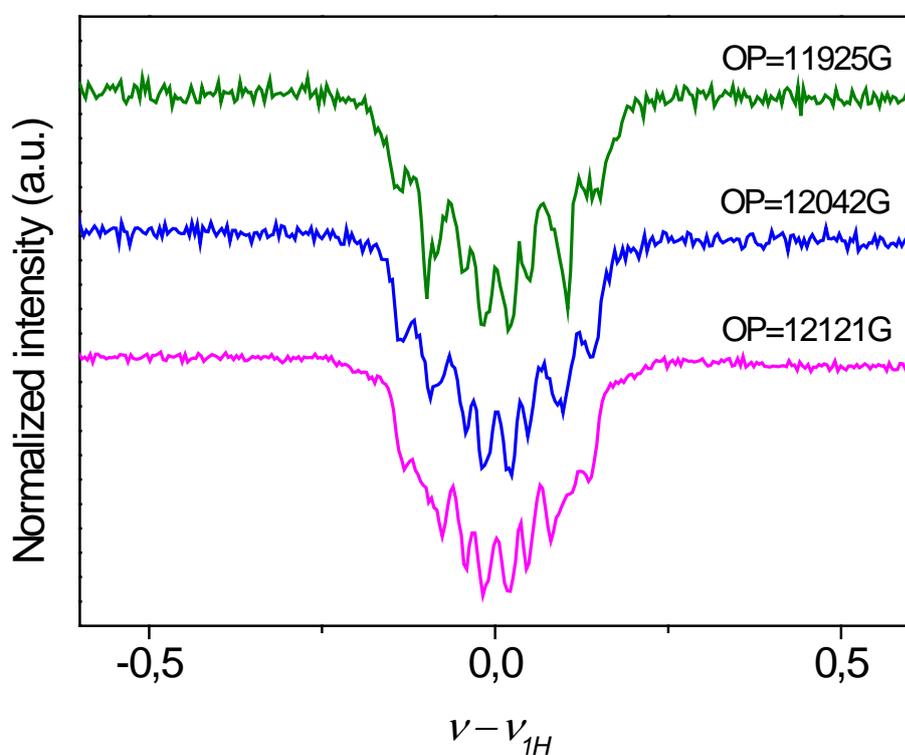

Figure Sx Q-band 1H Mims ENDOR spectra of V4+ ions measured at 10 K and different magnetic field settings.

We performed Mims ENDOR experiments to resolve small hf interactions between the V4+ centers and protons. The 1H

Mims ENDOR pattern recorded at different magnetic field settings at 10 K and is shown in Figure Sx.

At least four well resolved hf splittings can be observed indicating four protons in the vicinity of V4+.

Given the absence of direct chemical bonding between the V4+ ions and the protons, the isotropic contribution to the observed hf splittings is negligible (especially for the weaker couplings) and thus the point dipole approximation should be valid. We can thus use the following equation to estimate the V-H distances

$$T = \frac{\mu_0}{4\pi} g_e g_n \beta_e \beta_n \frac{1}{r^3}$$

with r being the distance between the unpaired electron localized in the V d orbitals and the ^{1}H nucleus and T the dipolar interaction directly measured from the ENDOR spectrum. The determined distances are 3.8(1), 4.3(1) 6.8(4) and 8.0(3) Å. Verificare se fittano con XRD